



Cite this: DOI: 10.1039/d3nj00099k

Palladium nanoparticles supported on reduced graphene oxide (Pd@rGO): an efficient heterogeneous catalyst for Suzuki–Miyaura, Heck–Matsuda and Double Suzuki–Miyaura cross-coupling reactions†

 Rajib Sarkar,^{id}^a Fillip Kumar Sarkar,^{id}^a Sushmita Gajurel,^{id}^a Lenida Kyndiah,^{id}^a Mithu Saha^b and Amarta Kumar Pal^{id}^{*a}

In the present work, we have developed a reduced graphene oxide (rGO)-supported palladium nanoparticle (Pd NP)-based nanocatalyst that can smoothly promote Suzuki–Miyaura and Heck–Matsuda coupling reactions from diazoarenes under base- and ligand-free conditions with low palladium loadings (ppm level). The as-synthesized catalyst (Pd@rGO) was comprehensively characterized by TEM, EDX, FT-IR, PXRD, TGA, ICP-OES and RAMAN analysis. Interestingly, the catalyst was also found to be effective in chemoselective double Suzuki–Miyaura cross-coupling reaction for the synthesis of various terphenyl derivatives in one-pot operation. The catalytic application of Pd@rGO was also extended to prepare Boscalid, a well-known fungicide. Additionally, the catalyst could be reused six times without much loss of activity.

 Received 7th January 2023,
 Accepted 5th May 2023

DOI: 10.1039/d3nj00099k

rsc.li/njc

Introduction

Pd-catalyzed coupling reactions are recognized as an essential tool in organic chemistry for the construction of carbon–carbon bonds.¹ The importance of Pd catalysis for coupling reactions was documented by the 2010 Nobel Prize in chemistry. Amongst various palladium-catalyzed cross-coupling reactions, Suzuki–Miyaura and Heck–Matsuda reactions have received considerable attention as they provide facile access to prepare biaryls and aryl-olefin compounds, which are an important core component present in various natural products and pharmaceuticals.^{2,3} Likewise, terphenyls are a group of aromatic hydrocarbon derivatives that exhibit diverse biological activities, such as potent immunosuppressive,⁴ cytotoxicity,⁵ neuroprotective,⁶ antitumor,⁷ antimicrobial,⁸ and 5-lipoxygenase inhibitory⁹ activities. Apart from these, they find applications in the construction of liquid crystals, molecular electronics, and fluorescent compounds.¹⁰ Fig. 1 shows some of the bioactive molecules containing biaryl and terphenyl moieties.

Over the years, halogenated and sulfonated electrophiles have been commonly used as the potential substrates in Suzuki–Miyaura and Heck–Matsuda coupling reactions.¹¹ However, arenediazonium salts are also reported as good alternative electrophiles towards these palladium catalyzed coupling reactions.¹² More specifically, they can be easily prepared from cheap and readily available arylamines and show better reactivity than expensive aryl halide and triflate surrogates used in these coupling reactions.¹³ Moreover, arenediazonium salts have been successfully employed in a number of palladium catalyzed coupling reactions and do not require the use of additional base and the reactions occur under mild conditions.¹⁴ Similarly, various dielectrophilic reagents such as 1-bromo-4-chlorobenzene,¹⁵ dibromobenzene,¹⁶ halo arenediazonium tetrafluoroborate,¹⁷ and potassium bromophenyltrifluoroborate¹⁸ salts have been utilized as building blocks for the synthesis of highly important terphenyl derivatives.

With the growing environmental concerns and economic issues, the development of cheap and reusable palladium catalysts for the coupling reactions has received significant interest. Although palladium-based homogeneous catalysts are efficient, they suffer from several drawbacks like the contamination of residual palladium species with the product and difficulty in removing the catalysts from the reaction media. Therefore, the development of a metal nanoparticle-based heterogeneous catalyst on a solid support with excellent recyclability and negligible metal leaching is highly desired.^{19–22} Over

^a Department of Chemistry, Centre for Advanced Studies, North-Eastern Hill University, Shillong, 793022, India. E-mail: amartya_pal22@yahoo.com, akpal@nehu.ac.in; Tel: +91 364 2307930 ext 2606

^b Department of Chemistry, Goalpara College, Goalpara, Assam, India

† Electronic supplementary information (ESI) available: The experimental details, spectral data of the products, and ¹H and ¹³C spectra of all products are available in the supporting information. See DOI: <https://doi.org/10.1039/d3nj00099k>

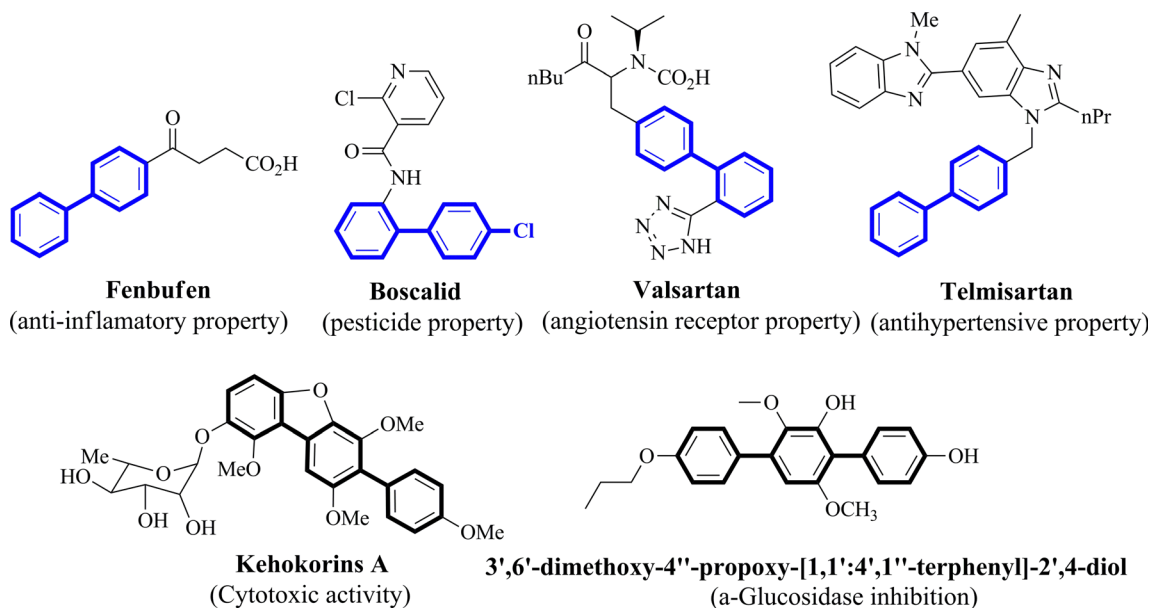


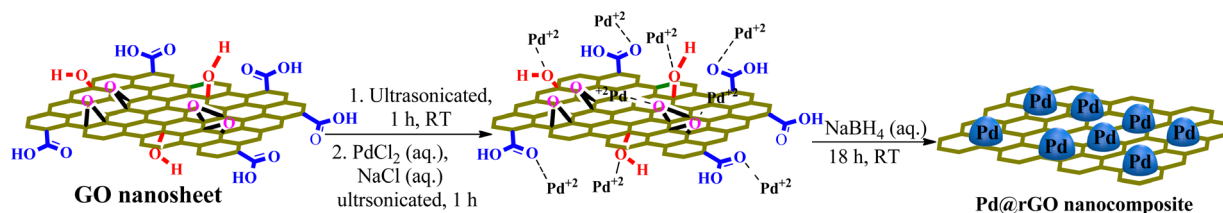
Fig. 1 Examples of some bioactive molecules containing a biaryl and terphenyl moiety.

the years, various palladium species like Pd organometallic complexes, Pd salts and Pd nanoparticles were attached or incorporated on different solid supports such as zeolite,²³ silica,²⁴ metal oxide,²⁵ polymer,²⁶ carbon²⁷ and metal-organic frameworks (MOFs)²⁸ to develop numerous palladium-based heterogeneous catalysts. Carbon-based materials such as activated carbon, carbon nanotubes, porous carbon, graphene, graphene oxide (GO), reduced graphene oxide (rGO), *etc.* have served as promising support materials in heterogeneous catalysis.²⁹ Among the various carbon-based materials, reduced graphene oxide (rGO) has gained increasing attention as a support material owing to its two-dimensional structure, large surface area, excellent stability and efficient electron mobility.^{30–33} Generally, GO and rGO are almost similar but GO is acidic in nature due to the presence of $-\text{COOH}$ functional groups. Therefore, sometimes it changes the P^H of the reaction medium, which hampers the reaction. On the other hand, rGO is almost neutral. So, this type of problem is absent in rGO catalyzed reactions. Furthermore, rGO is an inexpensive carbon material and easy to prepare from readily available graphite powder. In contrast, other carbon materials like carbon nanotubes are difficult to synthesize and costly. With the inspiration of the aforementioned advantages, we used reduced graphene oxide as a support material to anchor palladium nanoparticles to synthesize a Pd@rGO

nanocomposite catalyst and demonstrated its catalytic applications in the Suzuki–Miyaura and Heck–Matsuda coupling reactions using arenediazonium salts as an electrophile in methanol under mild, base-free, and ligand-free reaction conditions. Furthermore, we have also demonstrated chemoselective double Suzuki–Miyaura cross-coupling reaction in one-pot for the synthesis of various terphenyl derivatives. Moreover, we extended the catalytic application of Pd@rGO in Boscalid synthesis.

Results and discussion

The reduced graphene oxide supported palladium nanocomposite (Pd@rGO) was synthesized using a reduction protocol at room temperature and the detailed procedure is discussed in the Experimental section. The schematic representation showing the synthesis of the Pd@rGO catalyst is displayed in Scheme 1. The formation of the Pd@rGO catalyst was investigated by various analytical and spectroscopic techniques such as transmission electron microscopy (TEM), electron dispersive X-ray spectroscopy (EDX), powder X-ray diffraction (PXRD), inductively coupled plasma-optical emission spectroscopy (ICP-OES), X-ray photoelectron spectroscopy (XPS), FT-IR, Raman spectroscopy and thermogravimetric analysis (TGA).



Scheme 1 Schematic representation of the synthesis of the Pd@rGO nanocomposite.

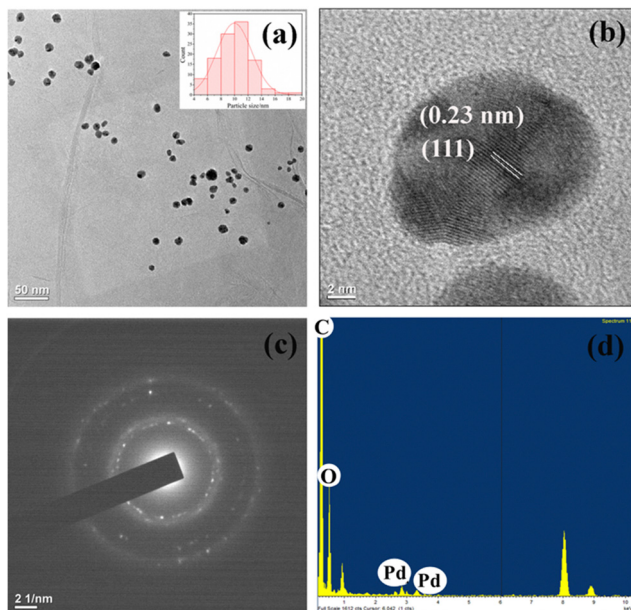


Fig. 2 (a) TEM image and particle size distribution of Pd@rGO (given in the inset). (b) HRTEM image, (c) SAED pattern and (d) EDX spectrum of Pd@rGO.

The distribution and size of the Pd nanoparticles on the rGO surface was investigated by TEM analysis (Fig. 2). The TEM image of Pd@rGO shows a uniform distribution of spherical Pd nanoparticles on the surface of rGO sheets (Fig. 2a). Furthermore, the high resolution TEM (HRTEM) image of a Pd nanoparticle on an rGO sheet revealed the lattice fringe distance of 0.23 nm, which correspond to the (111) plane of the face-centered cubic Pd (Fig. 2b).³³ The average size of the Pd nanoparticles was found to be 10 nm. The selected area electron diffraction (SAED) pattern of Pd@rGO displayed a spotty diffraction, which confirms the crystalline nature of the Pd NPs (Fig. 2c). The EDX spectrum of Pd@rGO showed the presence of C, O and Pd respectively (Fig. 2d). The Pd content in the Pd@rGO nanocomposite was determined by ICP-OES measurement, and it was found that

19.921 ppm of palladium was present in the 20 mg sample of Pd@rGO.

The XRD patterns of the synthesized GO, rGO and Pd@rGO are compared and shown in Fig. 3. The XRD pattern of GO shows a characteristic diffraction peak at $2\theta = 9.1^\circ$ and a small peak at $2\theta = 42.3^\circ$, corresponding to the (001) and (100) planes of the GO (Fig. 3a). In the XRD pattern of rGO, the disappearance of the peak at $2\theta = 9.1^\circ$ and the appearance of a broad peak at $2\theta = 24.6^\circ$ indicate that GO has been successfully reduced to rGO after the chemical reduction process (Fig. 3a). Furthermore, the XRD pattern of the Pd@rGO nanocomposite also shows the presence of a broad diffraction peak at $2\theta = 24.6^\circ$. The other characteristic diffraction peaks observed at 39.5° , 45.6° , and 66.7° , can be attributed to the (111), (200) and (220) crystalline planes of the face centered cubic structure of the Pd(0) nanoparticles (Fig. 3b).^{34,35}

The FT-IR spectra of GO, rGO and the Pd@rGO nanocomposite are shown in Fig. 4. The FT-IR spectrum of GO displays a broad absorption band at about 3400 cm^{-1} , which is due to the stretching vibration of the -OH group. The other characteristic peaks observed at 1098 , 1226 and 1392 cm^{-1} can be ascribed to the C-O alkoxy stretching, and C-O-C and C-OH stretching vibrations. The absorption bands at 1720 and 1628 cm^{-1} correspond to the -C=O stretching vibration and aromatic C=C stretching vibration, respectively. In the FT-IR spectrum of rGO, the broad peak of the O-H stretching vibrations slightly shifted to a higher wavenumber of 3419 cm^{-1} . A significant decrease in the intensities of the other peaks at 1105 and 1384 cm^{-1} was observed, indicating partial elimination of oxygen-containing functional groups after the reduction of GO to rGO (Fig. 4). Moreover, in the FT-IR spectrum of rGO and Pd@rGO, the carbonyl stretching frequency of the -COOH group at around 1720 cm^{-1} (observed in GO) almost vanished, which indicates the successful formation of rGO. It is also noted that the FT-IR spectra of rGO and Pd@rGO are almost similar, and not much change is observed (Fig. 4).³⁶

Raman spectroscopy is an essential tool for the characterization of carbon materials. Therefore, the transformation of

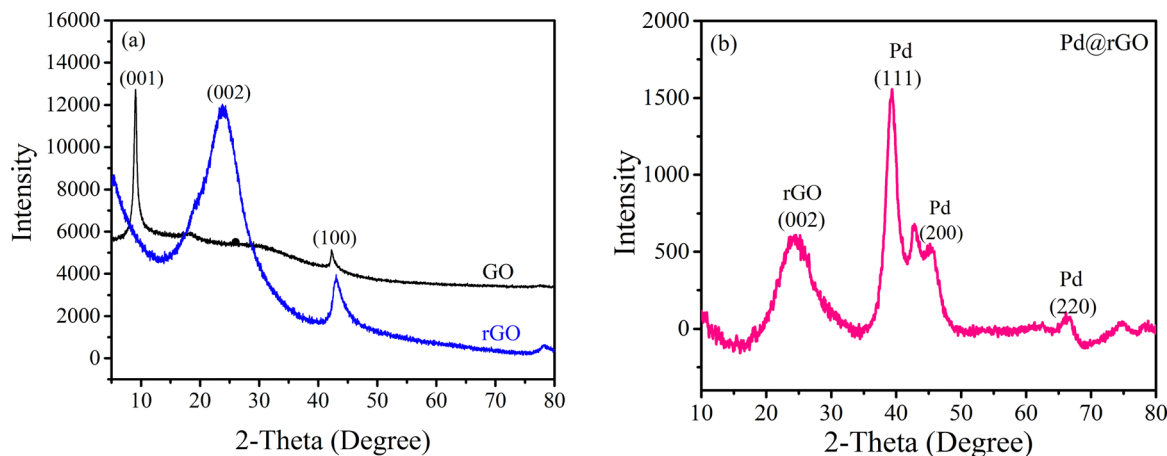


Fig. 3 PXRD patterns of (a) GO and rGO, and (b) Pd@rGO.

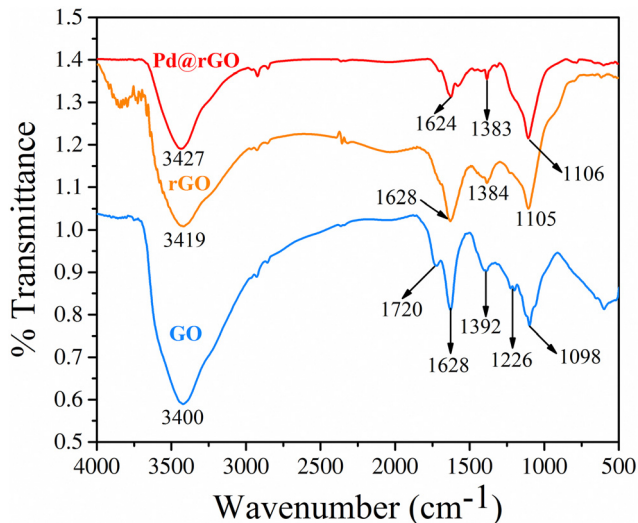


Fig. 4 FT-IR spectra of GO, rGO and the Pd@rGO nanocomposite.

GO to Pd@rGO was studied by Raman spectroscopy (Fig. 5a). Two characteristic peaks were observed in the Raman spectrum of GO. Namely, a G-band at around 1587 cm^{-1} and a D-band at around 1346 cm^{-1} , respectively. The G band is arising due to the in-plane vibration of the sp^2 carbon network and the D band reflects the defects and disorder in that network. The intensity ratio of the D and G bands (*i.e.* $I_{\text{D}}/I_{\text{G}}$ ratio) is related to the degree of disorder in graphitic materials. The $I_{\text{D}}/I_{\text{G}}$ value for Pd@rGO was found to be 1.19, which is lower than that of GO (1.26), indicating the increase in the degree of regularity in the carbon network after the reduction of GO to rGO.³⁷

Furthermore, the thermal stability of graphite, GO, rGO and Pd@rGO was evaluated by TGA analysis (Fig. 5b). The TGA curve of GO (red line) displays a weight loss of $\sim 20\%$ at around $100\text{ }^\circ\text{C}$, which can be attributed to the loss of intercalated H_2O molecules. A massive weight loss of $\sim 85\%$ at around $180\text{ }^\circ\text{C}$ was also observed, which can be ascribed to the decomposition of various oxygen-containing functional groups present in GO. On the other hand, the TGA thermograph of rGO displays a low

weight loss of $\sim 29\%$ at around $180\text{ }^\circ\text{C}$ as compared to GO ($\sim 85\%$). In comparison, Pd@rGO shows a similar weight loss of $\sim 38\%$ to that of rGO in the respective temperature range. This is due to the elimination of oxygenated functional groups from the surface of the Pd@rGO nanocomposite. Moreover, a slight increase in the thermal decomposition temperature was witnessed for the Pd@rGO nanocomposite because of strong interaction between rGO and palladium species. Furthermore, graphite (black line) shows almost negligible weight loss in the same experimental temperature range (Fig. 5b).^{34b,36a,38}

The oxidation state of palladium on the Pd@rGO nanocomposite was investigated by XPS analysis. As shown in Fig. 6, the XPS survey spectrum indicates the presence of carbon, oxygen and palladium elements in the as-synthesized Pd@rGO sample (Fig. 6a). The Pd 3d high resolution XPS spectrum shows two distinct peaks at 335.6 eV and 341.2 eV , corresponding to the metallic $\text{Pd}^0\text{ }3\text{d}_{5/2}$ and $\text{Pd}^0\text{ }3\text{d}_{3/2}$ transitions, respectively. In addition, the two peaks observed at 333.5 eV and 338.8 eV can be ascribed to the $\text{Pd}^{2+}\text{ }3\text{d}_{5/2}$ and $\text{Pd}^{2+}\text{ }3\text{d}_{3/2}$, respectively (Fig. 6b). The ratio between metallic Pd and Pd^{2+} species is 1:1.13. Therefore, it can be concluded that a mixture of both Pd(0)/Pd(+2) is involved in catalyzing the cross-coupling reactions.³⁹

Suzuki–Miyaura cross-coupling

After the successful preparation of Pd@rGO nanocomposites, we studied the catalytic activity of Pd@rGO for the Suzuki–Miyaura cross-coupling reaction, which is most frequently used to synthesize pharmaceutical intermediates and fine chemicals.

Even though arenediazonium salts have been well established as effective coupling partners in Pd-catalyzed reactions, but most of them are generally unstable. In contrast, arenediazonium tetrafluoroborates are considered ideal coupling partners for Suzuki–Miyaura coupling reaction as they show remarkably improved stability over other arenediazonium salts with more nucleophilic counter ions.⁴⁰ To optimize the reaction conditions for Suzuki–Miyaura cross-coupling reaction, 4-nitroarenediazonium

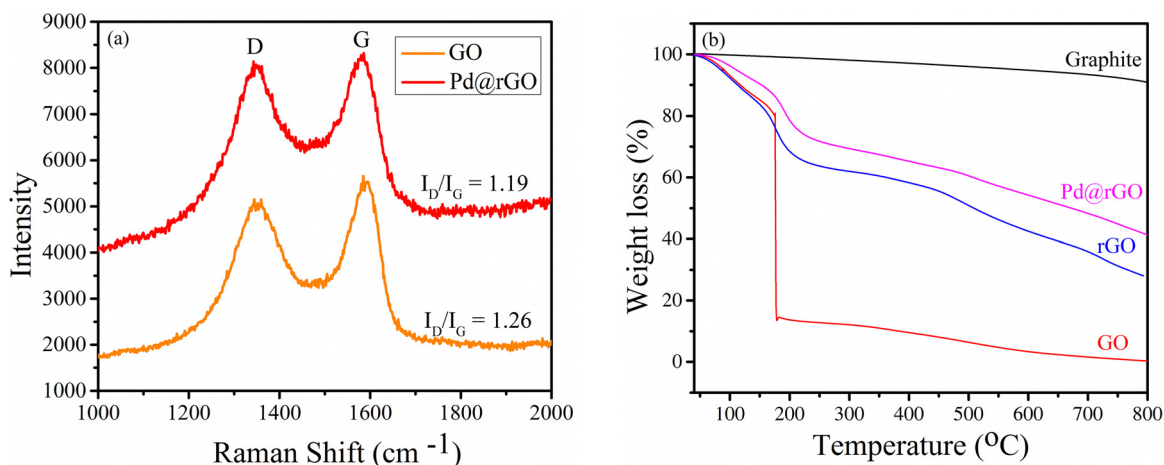


Fig. 5 (a) Raman spectra of GO and Pd@rGO. (b) TGA thermographs of graphite, GO, rGO and Pd@rGO.

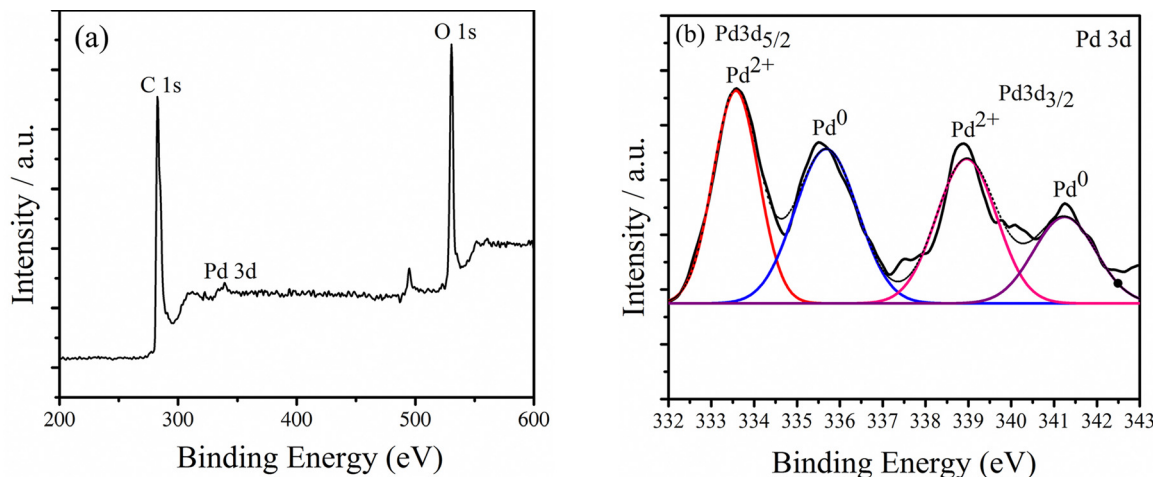


Fig. 6 (a) XPS survey spectrum and (b) high-resolution spectrum of the Pd 3d core level of Pd@rGO.

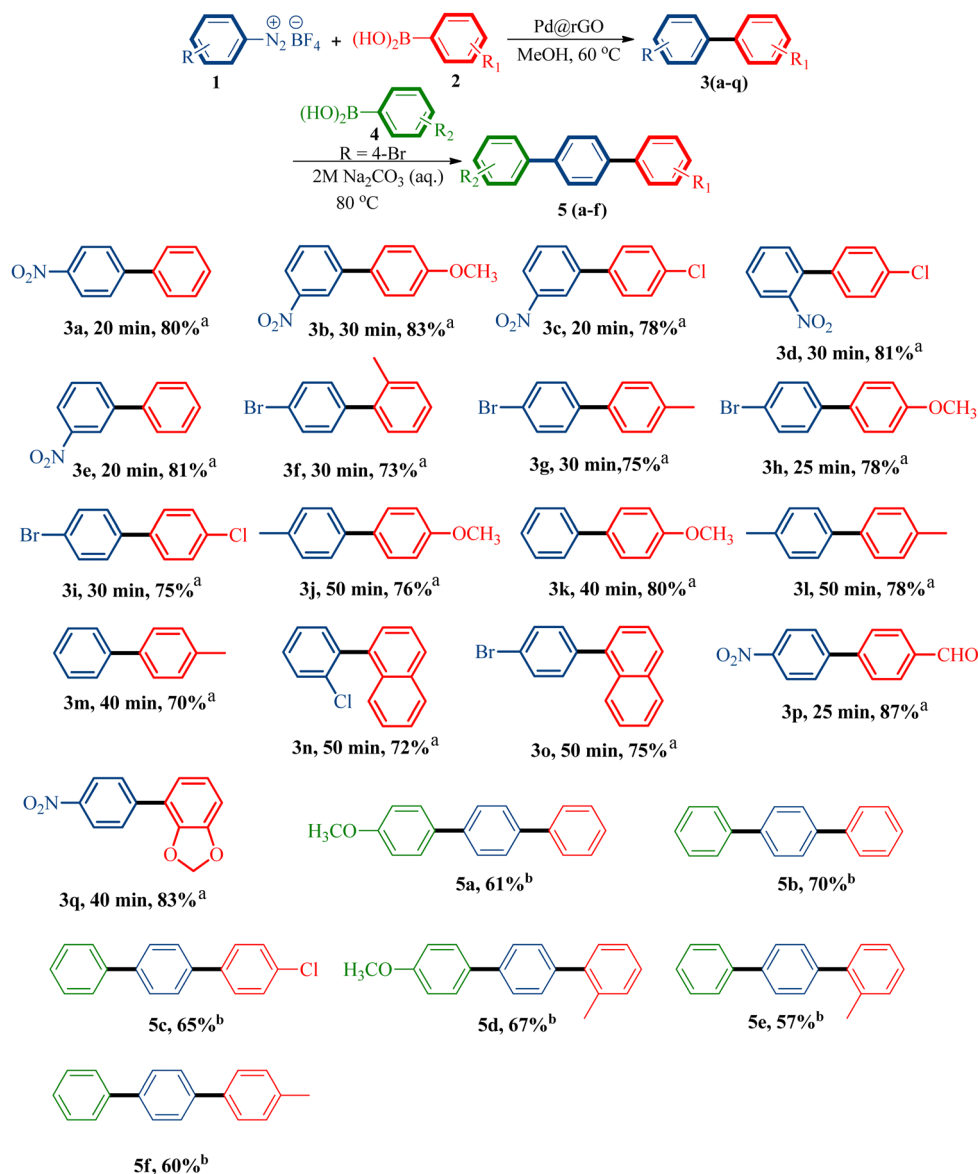
tetrafluoroborate **1a** and phenylboronic acid **2a** were chosen as the coupling partners (Table 1). Initially, we screened a variety of solvents such as H₂O, ethanol (EtOH), methanol (MeOH), isopropanol (i-PrOH), 1,4-dioxane, CH₃CN and DMF at moderate temperature (60 °C) using 20 mg of Pd@rGO as the catalyst (Table 1, entries 1–7). The maximum yield (80%) of the biaryl product (**3a**) was obtained in MeOH as solvent (Table 1, entry 3). Other solvents provided inferior yields of the desired products (Table 1, entries 1, 2, 4, 5, 6 and 7). The model reaction was also performed in solvent-free reaction conditions, but the reaction did not furnish the desired product and the starting materials remained unreacted (Table 1, entry 8). The effect of different temperatures (25, 40, 50, 60 and 70 °C) on the model reaction was also studied. It was found that, the yield of the product

increased with the increase in reaction temperature and the best result was achieved at 60 °C (Table 1, entries 3, 12–14); a further increase in the reaction temperature (70 °C) did not provide higher yield (Table 1, entry 15). Next, the effect of different amounts of catalyst loading on the synthesis of the desired product (**3a**) was examined. The yield of the product was increased from 54% to 80% with the rise of Pd@rGO loading from 10 to 20 mg (Table 1, entries 3, 9–10). However, no significant improvement in the yield of the product was observed when the amount of catalyst increased from 20 to 25 mg (Table 1, entries 3 and 11). The model reaction was also tested with commercial Pd(OAc)₂ and Pd/C as catalysts, but only 38% and 76% yield of the product was obtained at 60 °C (Table 1, entries 17 and 18). Next, the model reaction was

Table 1 Optimization of the Suzuki–Miyaura reaction^a

Entry	Catalyst (mg)	Solvent	Temp. (°C)	Time (min)	Product	Yield ^b (%)
1	Pd@rGO (20)	H ₂ O	Reflux	720	3a	17
2	Pd@rGO (20)	EtOH	60	20	3a	74
3	Pd@rGO (20)	MeOH	60	20	3a	80
4	Pd@rGO (20)	i-PrOH	60	20	3a	67
5	Pd@rGO (20)	1,4-dioxane	60	20	3a	65
6	Pd@rGO (20)	CH ₃ CN	60	20	3a	37
7	Pd@rGO (20)	DMF	60	20	3a	72
8	Pd@rGO (20)	Solvent free	60	20	3a	—
9	Pd@rGO (10)	MeOH	60	20	3a	54
10	Pd@rGO (15)	MeOH	60	20	3a	68
11	Pd@rGO (25)	MeOH	60	20	3a	80
12	Pd@rGO (20)	MeOH	25 (r.t)	1440	3a	67
13	Pd@rGO (20)	MeOH	40	20	3a	53
14	Pd@rGO (20)	MeOH	50	20	3a	69
15	Pd@rGO (20)	MeOH	70	20	3a	80
17	Pd(OAc) ₂ (1)	MeOH	60	20	3a	38
18	Pd/C (20)	MeOH	60	20	3a	76
19	Catalyst-free	MeOH	60	20	3a	—

^a Reaction conditions: arenediazonium salt **1a** (1.2 mmol), boronic acid **2a** (1 mmol) were allowed to react in the presence of catalyst and solvent (5 ml). ^b Isolated yield.

Table 2 Substrate scope of Pd@rGO-catalyzed Suzuki–Miyaura^a and double Suzuki–Miyaura^b cross-coupling reaction

^a Reaction conditions: arenediazonium salt **1** (1.2 mmol), boronic acid **2** (1 mmol), Pd@rGO (20 mg) and MeOH (5 ml) were stirred at 60 °C.

^b Reaction conditions: in the first step, 4-bromoarenediazonium tetrafluoroborate **1e** (1.2 mmol), arylboronic acid **2** (1 mmol) and Pd@rGO (30 mg) were mixed in methanol (5 ml) and stirred for 1 h at 60 °C. In the second step, 2 M aqueous Na₂CO₃ (2 ml) and arylboronic acid **4** (1.2 mmol) were added dropwise and the mixture was stirred for 6 h at 80 °C.

conducted without catalyst, but the product **3a** was not detected in the reaction mixture, and only starting materials were witnessed. This result confirms the role of palladium in the coupling reaction (Table 1, entry 19). Therefore, 20 mg of the Pd@rGO catalyst was used in the subsequent experiments to prepare biaryl products in methanol at 60 °C.

Encouraged by this result, the substrate scope of this Suzuki–Miyaura coupling reaction was investigated in the next step under the optimized reaction conditions and the results are summarized in Table 2. A wide variety of arenediazonium tetrafluoroborate salts bearing electron-withdrawing and electron-donating groups were examined. Arenediazonium tetrafluoroborates containing electron-withdrawing groups such

as chloro (–Cl), bromo (–Br), and nitro (–NO₂) groups at the *ortho*, *meta* and *para* positions in the benzene ring, underwent the reactions smoothly within short reaction times to give the desired products in high yields (Table 2). Arenediazonium salts containing electron-donating groups such as methyl (–CH₃) functional groups also reacted smoothly but require slightly longer reaction time in delivering the products **3j** and **3l**, in 76% and 78% yields, respectively. The scope of the various boronic acids was explored and it was found that phenylboronic acids bearing methyl (–CH₃), methoxy (–OCH₃), chloro (–Cl) and aldehyde (–CHO) functional groups were well tolerated in the reaction, leading to the formation of the corresponding products in moderate to good yields (Table 2). Also, for the

phenylboronic acid bearing a methyl ($-\text{CH}_3$) group at the *ortho* position of the benzene ring, a good yield of 73% of the product **3f** was achieved. The reactions employing unsubstituted phenylboronic acid were also found to be compatible and furnished the biaryl products **3a** and **3e** in 80% and 81% yields. Moreover, relatively bulky 1-naphthalene boronic acid was found to be suitable for the reaction and afforded the desired products **3n** and **3o** in 72% and 75% yields. A slightly complicated boronic acid like 3,4-(methylenedioxy)benzeneboronic acid also reacted smoothly and gave the corresponding biaryl **3q** in 83% yield. Therefore, irrespective of the electronic and steric nature of the coupling partners, the cross-coupling reaction progressed very fast and produced the corresponding coupling products in good to high yields under very short reaction times.

After successful demonstration of the Suzuki–Miyaura cross-coupling of arenediazonium tetrafluoroborate salts with arylboronic acids under base-free and ligand-free conditions, we next carried out the chemoselective double Suzuki–Miyaura cross-coupling of arenediazonium tetrafluoroborate salts with arylboronic acids (Table 2). After some optimization of the reaction conditions, the developed Pd@rGO catalyst was found to be active for the sequential chemoselective double Suzuki–Miyaura cross-coupling reactions in one-pot, which led to the formation of various terphenyl derivatives in moderate to good yields. Initially, the first coupling was conducted with 4-bromoarenediazonium tetrafluoroborate and arylboronic acid **2** at 60 °C in methanol to furnish the bromo-containing biaryl product. Then, this product was subjected directly to the second coupling with another boronic acid **4** in the same pot in the presence of aq. Na_2CO_3 at 80 °C and the reaction took place at the C–Br bond to obtain the desired terphenyls **5 (a–f)** (Table 2).

Heck–Matsuda coupling

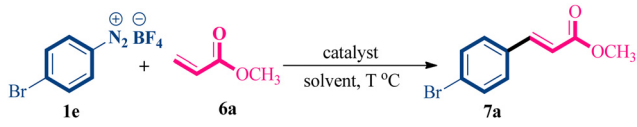
The application of the Pd@rGO nanocatalyst was further evaluated for the Heck–Matsuda C–C coupling reaction among

arenediazonium tetrafluoroborate salts and acrylates. For optimization, the reaction between 4-bromobenzenediazonium tetrafluoroborate salt and methyl acrylate in the presence of the Pd@rGO (25 mg) catalyst was selected as the model reaction. Then, the model reaction was performed in different solvents such as H_2O , EtOH, MeOH, *i*-PrOH and 1,4-dioxane (Table 3, entries 1–5). The maximum yield of the product **7a** was obtained in methanol (Table 3, entry 3). The reaction in solvent-free conditions produced poor yield of the coupling product (Table 3, entry 11). Next, the effect of different temperatures including 25 (r.t.), 40, 50 and 60 °C on the model reaction was investigated (Table 3, entries 3, 8–10). The best result was obtained at 50 °C (Table 3, entry 3). Increasing the temperature to 60 °C did not significantly increase the product yield (Table 3, entry 8), whereas lowering the temperature afforded poor yield of the product (Table 3, entries 9 and 10). We noticed that 25 mg of the catalyst offered the highest yield. However, low catalyst loading executed lower yields but more than 25 mg of catalyst was unable to generate a yield higher than 70% (Table 3, entries 3, 6, and 7). Furthermore, the model reaction was unsuccessful in producing any coupling product without the catalyst (Table 3, entry 12).

With the optimized reaction conditions in hand, we next explored the scope and generality of this protocol. From Table 4, it is clear that benzenediazonium tetrafluoroborates with electron-donating and electron-withdrawing groups reacted well with both methyl acrylate and ethyl acrylate and offered moderate to good yields of the coupling products (**7a–7i**). Better yields of the desired products were obtained when the benzenediazonium tetrafluoroborates carried electron-withdrawing groups such as NO_2 , Cl and Br (Table 4). It is worth mentioning that the established reaction conditions show very high chemoselectivity because the coupling reaction takes place at the diazonium portion even in the presence of halogens (Br and Cl).

We further applied our developed catalyst (Pd@rGO) for the synthesis of Boscalid, a well-known fungicide marketed by BASF Company (Scheme 2).⁴¹ The crucial step of Boscalid

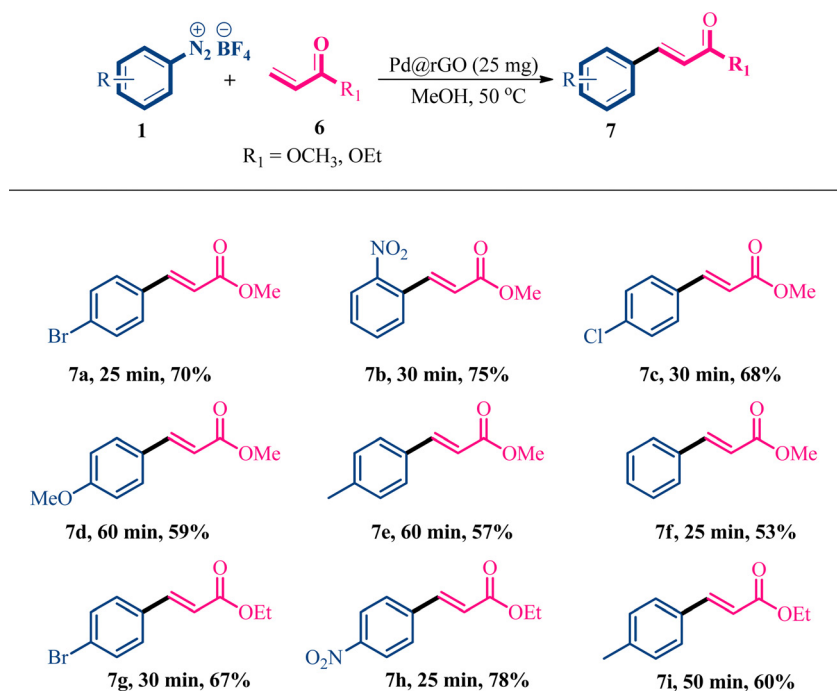
Table 3 Optimization of the Heck–Matsuda reaction with the Pd@rGO catalyst^a



Entry	Catalyst (mg)	Solvent	Temp. (°C)	Time (min)	Product	Yield ^b (%)
1	Pd@rGO (25)	H_2O	Reflux	720	7a	—
2	Pd@rGO (25)	EtOH	50	25	7a	48
3	Pd@rGO (25)	MeOH	50	25	7a	70
4	Pd@rGO (25)	<i>i</i> -PrOH	50	25	7a	57
5	Pd@rGO (25)	1,4-dioxane	50	25	7a	18
6	Pd@rGO (20)	MeOH	50	25	7a	54
7	Pd@rGO (30)	MeOH	50	25	7a	70
8	Pd@rGO (25)	MeOH	60	25	7a	70
9	Pd@rGO (25)	MeOH	40	25	7a	56
10	Pd@rGO (25)	MeOH	25	25	7a	32
11	Pd@rGO (25)	Solvent-free	50	25	7a	57
12	Catalyst-free	MeOH	50	25	7a	—

^a Reaction conditions: 4-bromobenzenediazonium tetrafluoroborate **1e** (1.2 mmol), methyl acrylate **6a** (1 mmol), catalyst and solvent (5 ml) were stirred at 50 °C. ^b Isolated yield.

Table 4 Substrate scope of Pd@rGO catalyzed Heck–Matsuda reaction



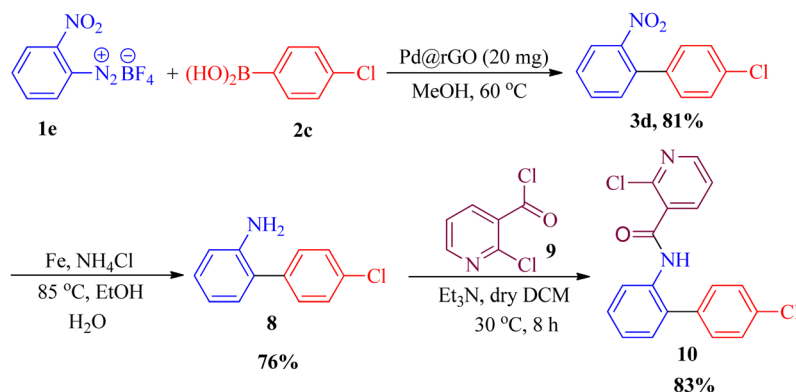
Reaction conditions: arenediazonium salt **1** (1.2 mmol), methyl/ethyl acrylate **6** (1 mmol), Pd@rGO (25 mg) and MeOH (5 ml) were stirred at 50 °C.

synthesis is the making of substituted biaryl (**3d**) by palladium catalyzed Suzuki–Miyaura coupling reaction. It is considered that the largest application of the Suzuki–Miyaura coupling reaction is for producing Boscalid at an industrial level. So, a huge amount of palladium catalyst is used for the said synthesis, which makes the procedure very costly. Here we used our designed Pd@rGO catalyst (20 mg) under the above-mentioned optimized reaction conditions. The Pd@rGO catalyst showed brilliant efficiency in producing the biaryl **3d** in high yield (81%). Moreover, the Pd@rGO catalyst can be easily separated from the reaction mixture by centrifugation followed by filtration, which is the main advantage from the industrial point of view. Then, the reduction of the nitro group (**3d**), and

subsequent condensation with 2-nicotinylchloride (**9**) furnished the desired boscalid (**10**) in 83% yield.

Catalyst recycling study

The recoverability and reusability of the Pd@rGO catalyst were investigated for the Suzuki–Miyaura reaction. The coupling of 4-nitrobenzenediazonium tetrafluoroborate (**1a**) with phenylboronic acid (**2a**) was carried out in 2 mmol scale in the presence of Pd@rGO under the optimal reaction conditions. After completion of the reaction, the catalyst was recovered by centrifugation and filtration, and then it was washed with DCM



Scheme 2 Synthesis of boscalid using Pd@rGO as a catalyst.

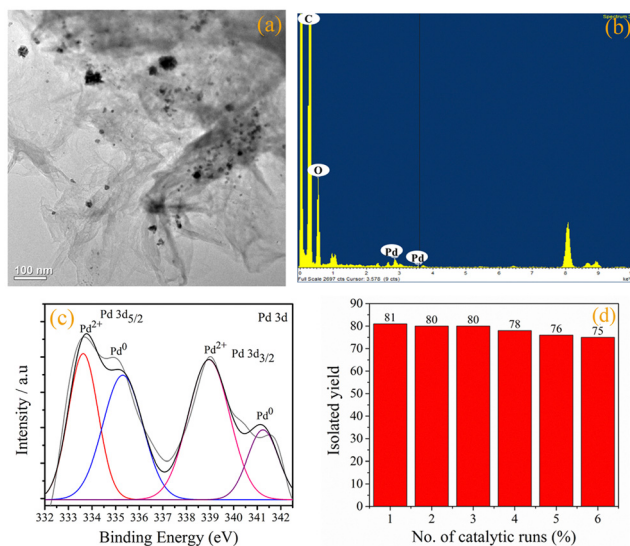


Fig. 7 (a) TEM image, (b) EDX spectrum and (c) XPS spectrum of the Pd 3d core level of the reused Pd@rGO catalyst, and (d) reusability chart of the Pd@rGO catalyst.

(3 × 10), dried at 40 °C for 12 h and directly used in the next cycle of reaction. As shown in Fig. 7d, the Pd@rGO catalyst displayed almost constant catalytic activity up to six consecutive cycles with a slight decrease in the product yield. The TEM image of the reused Pd@rGO revealed that not much significant change occurred in the morphology, and only a small amount of palladium nanoparticles agglomerated on the surface of the rGO sheets, which may be the reason for the slight decrease in the product yield during the recycling process (Fig. 7a). The EDX spectrum shows the presence of C, O and Pd elements in the reused Pd@rGO catalyst (Fig. 7b). Furthermore, the high-resolution XPS spectrum of the Pd 3d core level of the recycled

Pd@rGO catalyst after the sixth cycle of reaction is shown in Fig. 7c. The Pd 3d spectrum of the recycled catalyst shows two characteristic components consisting of Pd 3d_{5/2} and Pd 3d_{3/2}, respectively (Fig. 7c). The peaks at 335.2 and 341.2 eV could be ascribed to metallic Pd⁰, while the other peaks observed at 333.6 and 338.9 eV could be assigned to Pd²⁺ species. Therefore, a mixture of both Pd(0)/Pd(+2) is present in the recycled Pd@rGO catalyst. These results are in good agreement with the data of the fresh Pd@rGO catalyst.

Hot filtration and mercury tests for the Pd@rGO catalyst

In order to investigate the amount of Pd leached into the reaction medium, a hot filtration test was performed for the Suzuki–Miyaura coupling reaction. For this experiment, 4-nitrobenzenediazonium tetrafluoroborate **1a**, phenyl boronic acid **2a** and Pd@rGO (20 mg) were used under the optimum reaction conditions. After 10 min of stirring, the catalyst was separated and the reaction was further continued for another 10 min. No change in the yield of the product was witnessed after the separation of the catalyst. This in turn proved that either no leaching or negligible leaching of palladium from the Pd@rGO catalyst occurred. Moreover, ICP-OES analysis of the reaction solution also displayed very negligible leaching of palladium (0.199 ppm). A mercury (Hg) drop experiment was then carried out to ensure the heterogeneity of the Pd@rGO catalyst. When a drop of mercury (60 mg) was added to the model reaction of Suzuki–Miyaura cross-coupling reactions under the optimized reaction conditions, and only a trace amount of the product was formed after 20 min. This is because Hg poisons the surface of the Pd@rGO catalyst and hence reduces its catalytic activity. These results indicate the true

Table 5 Comparison of the catalytic activity of Pd@rGO with previously reported catalysts for Suzuki–Miyaura coupling reaction

Entry	Catalyst	Reaction conditions	Yield (%)	Ref.
1	NiCl ₂ -glyme (10 mol%)	Glycerol, DMSO, 80 °C, 12 h	70–90	43
2	Pd@NPA ₂ -1.0 (1.3–5.4 mg)	<i>i</i> -PrOH/H ₂ O, K ₂ CO ₃ , 100 °C, under argon, 6–18 h	90–100	44
3	Pd@CQD@Fe ₃ O ₄ NPs (0.3 mol%)	<i>t</i> -BuOK, EtOH-H ₂ O (1 : 1), 60–120 °C, 1–24 h	75–100	45
4	Pd-MOF (3 mol%)	MeOH, 40 °C, 2–8 h	46–98	46
5	PdCl ₂ (PPh ₃) ₂ (0.3 mol%)	K ₂ CO ₃ , Toluene, H ₂ O, 110 °C, N ₂ , 2–12 h	15–98	47
6	Ni(PCy ₃) ₂ Cl ₂ (6 mg)	PCy ₃ , Cs ₂ CO ₃ , Toluene, 150 °C, N ₂ , 24 h	42–88	48
7	Na ₂ [Pd-(BuHSS)] (0.1 mol%)	Cs ₂ CO ₃ , H ₂ O, 80 °C, 2 h	70–92	49
8	Pd-Fe ₃ O ₄ -PTB (0.04% mol)	K ₂ CO ₃ (2.5 mmol), MI 400 W, 5 min	62–98	50
9	Pd@COF-QA (1.7 mol%)	Et ₃ N, H ₂ O, 50 °C, 6 h	42–99	51
10	Pd(OAc) ₂ (8 mol%)	Ag ₂ CO ₃ , H ₂ O:EtOH (2 : 1), N ₂ , 5 h, 60 °C	41–77	52
11	Pd@rGO (20 mg)	MeOH, 60 °C, 20–50 min	70–87	This Work

Table 6 Comparison of the catalytic activity of Pd@rGO with previously reported catalysts for Heck–Matsuda coupling reaction

Entry	Catalyst	Reaction conditions	Yield (%)	Ref.
1	Pd@CS/PAAS nanofiber (25 mg)	Et ₃ N, DMAc, 110 °C, 3–24 h	28–98	53
2	MNPs-Mel-Pd (10 mg)	Et ₃ N, DMSO, 100 °C, 0.5–6 h	65–98	54
3	POLITAG-Pd ⁰ -HM (10 wt%)	Et ₃ N, GVL, 150 °C, 8 h	78–99	55
4	MOPs-Pd-I (50 mg)	Et ₃ N, DMF, 120 °C, 1.5 h	90–98	56
5	Fe ₃ O ₄ @HcdMeen-Pd(0) (0.30 mol%)	Cs ₂ CO ₃ , H ₂ O, 100 °C, 15–160 min	67–99	57
6	Pd@rGO (20 mg)	MeOH, 60 °C, 20–50 min	53–78	This Work

heterogeneous nature of the catalyst in the course of the reaction.⁴²

To examine the efficiency of our catalyst, we compared the results of the Suzuki–Miyaura and Heck–Matsuda coupling reactions with the previously reported Pd-catalysts. Tables 5 and 6 show that the present catalytic protocols display better performance than the other reported systems in terms of base free conditions, ambient reaction conditions, and shortest reaction time for the synthesis of the coupling products.

Conclusion

In conclusion, we have developed an efficient synthetic methodology for the Pd@rGO catalyzed Suzuki–Miyaura and Heck–Matsuda cross-coupling reactions using arene diazonium tetrafluoroborate salts as electrophiles under mild reaction conditions. We also took further advantage of the present protocol to synthesize various terphenyl derivatives *via* a chemoselective double Suzuki–Miyaura cross-coupling reaction in one-pot. More interestingly, the synthesized Pd@rGO catalyst can also be applied for the synthesis of boscalid, a well-known fungicide, clearly supporting the advantage of the present protocol. Additionally, mild reaction conditions, use of non-toxic solvent, moderate reaction temperature, low palladium loading and easy recovery and reusability of the catalyst at least six times are some of the significant advantages of the present work.

Experimental section

All the necessary chemicals required were purchased from Sigma-Aldrich, Alfa Aesar and Spectrochem and utilized without further purification. IR spectra were recorded on a Bruker Alpha II system (ν_{\max} in cm^{-1}) on KBr disks. ^1H NMR and ^{13}C NMR (400/500 MHz and 100/125 MHz, respectively) spectra were recorded on a Bruker Avance II-400 spectrometer in CDCl_3 (chemical shifts in δ with TMS as internal standard). GC-MS spectra were recorded on an Intuvo 9000GC System & 5977B GC/MSD, Agilent instrument. ESI-mass spectra were recorded on a Xevo TQ-XS, Water Mass Spectrometer. Transmission Electron Microscopy (TEM) and Energy Dispersive X-ray (EDX) analysis were recorded on a JEM-2100, 200 kV, Jeol. Powder XRD was recorded on a BRUKER AXS, D8 FOCUS instrument. Inductively Coupled Plasma-Optical Emission Spectrometry (ICP-OES) was carried out on a Thermo Scientific™ iCAP™ 7600 instrument. Thermogravimetric analysis (TGA) was recorded on a PerkinElmer Precisely STA 6000 simultaneous thermal analyzer. Raman analysis was carried out on a Renishaw Basis Series with 514 lasers. X-Ray Photoelectron Spectroscopy (XPS) was performed using a PHI 5000 VersaProbe III instrument.

Synthesis of Graphite Oxide (GO)

GO was prepared according to the reported procedure from graphite powder.⁵⁸ Typically, 1 g of graphite powder and 0.5 g of sodium nitrate were added to 20 ml of concentrated H_2SO_4

(98%), and the mixture was kept in an ice-bath and stirred for 30 min. Next, 6 g of KMnO_4 was slowly added in portions over a period of 1 h, and the mixture was stirred again in an ice-bath for another 1 h. The temperature of the mixture was then brought slowly to 35 °C (± 5 °C) and stirred for 1 h. After 1 h stirring, 20 ml of de-ionized water was added to the mixture and continued to stir at 35 °C (± 5 °C) for another 30 min. Finally, 180 ml of de-ionized water was added to the mixture followed by dropwise addition of H_2O_2 (30%), which resulted in the formation of a bright yellow suspension. The synthesized graphite oxide was then collected by centrifugation, and washed three times with water (3×30 ml) followed by ethanol (3×30 ml) and diethyl ether (3×30 ml). Finally, the obtained graphite oxide was dried in an oven at 40 °C for 24 h.

Synthesis of Pd@rGO

In a 250 ml round bottom flask, GO (1 g) was dispersed in DI water (100 ml) and ultrasonicated for 1 h at room temperature. After that, an aqueous solution of PdCl_2 (0.02 M, 5 ml) and NaCl (0.05 M, 5 ml) was added and the resulting reaction mixture was further ultrasonicated at room temperature for another 1 h. Next, a freshly prepared aqueous solution of NaBH_4 (3 ml, 0.5 M) was added to the above suspension and stirred for 18 h at room temperature (25 °C). The prepared Pd@rGO catalyst was collected by centrifugation and filtration, and washed three times with H_2O (3×30 ml) followed by ethanol (3×20 ml) and diethyl ether (3×10 ml). Finally, the obtained Pd@rGO catalyst was dried at 40 °C for 24 h.

General procedure for the synthesis of arenediazonium tetrafluoroborates

An appropriate arylaniline (10 mmol) was dissolved in a mixture of hydrofluoroboric acid (3.4 ml) and distilled water (4 ml). The reaction mixture was cooled to 0 °C using an ice-bath, and then an aqueous solution of sodium nitrite (0.69 g in 1.5 ml of water) was added dropwise. After stirring for 40 min at 0–5 °C, the obtained precipitate was collected by filtration, dried and redissolved in a minimum amount of acetone. Then, the product was again precipitated by slow and dropwise addition of diethyl ether with vigorous stirring. Finally, the product was filtered, washed several times with small portions of diethyl ether, and dried under vacuum.

General procedure for the synthesis of biaryls (3a–3q) and terphenyl derivatives (5a–5f)

A mixture of arenediazonium tetrafluoroborate salt (1, 1.2 mmol), arylboronic acid (2, 1 mmol), and Pd@rGO (20 mg) in MeOH (5 ml) was stirred at 60 °C for the time indicated in Table 2. After completion of the reaction (TLC), the reaction mixture was cooled and the catalyst was removed by centrifugation followed by filtration. The recovered catalyst was washed with DCM (3×5 ml), dried at 40 °C for 12 h and directly used in the next cycle of reaction. The organic filtrate was concentrated and the resulting residue was purified by column chromatography over silica gel (60–120 mesh) by using ethyl acetate in hexane (0–10%) as an eluent to obtain the pure products. To prepare the

terphenyls, a mixture of 4-bromoarenediazonium tetrafluoroborate (1.2 mmol), arylboronic acid (**2**, 1 mmol), Pd@rGO (30 mg) and MeOH (5 ml) was stirred at 60 °C for 1 h. Next, aqueous Na₂CO₃ solution (2 M, 2 ml) and the second arylboronic acid (**4**, 1.2 mmol) were added slowly to the same reaction vessel and the reaction mixture was allowed to stir for another 6 h at 80 °C. The catalyst was then separated by centrifugation followed by filtration. The organic solvent was then removed from the filtrate by evaporation and the aqueous layer was extracted by dichloromethane (3 × 5 ml), washed with water (3 × 5 ml) and brine (1 × 5 ml), and dried over anhydrous sodium sulphate. Finally, the dichloromethane was removed and the crude product was purified by column chromatography (silica gel 60–120 mesh) by using ethylacetate in hexane as an eluent to afford the desired products.

General procedure for the synthesis of cinnamates (7a–7i)

A mixture of arenediazonium tetrafluoroborate salt (**1**, 1.2 mmol), acrylate (**6**, 1 mmol) and Pd@rGO (25 mg) in MeOH (5 ml) was stirred at 50 °C for the time mentioned in Table 4. After completion of the reaction (TLC), the reaction mixture was cooled at room temperature and the catalyst was separated by centrifugation followed by filtration. The filtrate was concentrated to dryness by evaporation. Finally, the resulting residue was purified by column chromatography over silica gel by using ethyl acetate and hexane as an eluent to obtain the respective products.

Synthesis of 4-chloro-2'-nitrobiphenyl (3d)

Synthesis of 4-chloro-2'-nitrobiphenyl (**3d**) was carried out by following the general procedure for the synthesis of biaryls (**3a–3q**).

Synthesis of 2-amino-4'-chlorobiphenyl (8)

Typically, Fe powder (2.75 mmol), NH₄Cl (0.5 mmol) and H₂O (1 ml) were added to a solution of 4-chloro-2'-nitrobiphenyl (**3d**, 1 mmol) in EtOH (5 ml), and the resulting mixture was magnetically stirred for 1 h at 85 °C. After that, the reaction was cooled to room temperature and the organic solvent was removed from the reaction mixture. The aqueous layer was extracted by dichloromethane (3 × 5 ml), washed with water (3 × 5 ml) and brine (1 × 5 ml), and dried over anhydrous sodium sulphate. Finally, the dichloromethane was removed and the crude product was purified by column chromatography (silica gel 60–120 mesh) by using ethyl acetate and hexane as an eluent to afford the desired product **8**.

Synthesis of 2-chloronicotinoyl chloride (9)

To a solution of chloronicotinic acid (1 mmol) in dry dichloromethane (5 ml), (COCl)₂ (2 mmol) and DMF (0.2 ml) were added and the mixture was stirred at 25 °C for 5 h under a nitrogen atmosphere. After completion of the reaction, the solvent was removed under reduced pressure. Then, the crude product was used for the synthesis of boscalid without further purification.

Synthesis of boscalid (10)

Typically, Et₃N (0.5 mmol) and 2-amino-4'-chlorobiphenyl (**8**, 0.5 mmol) were added to a solution of 2-chloronicotinoyl

chloride (**9**, 0.75 mmol) in dry dichloromethane (3 ml) under N₂ atmosphere. The reaction mixture was then stirred at 30 °C for 8 h under a N₂ atmosphere. After completion of the reaction time, 10 ml of water was added to the reaction mixture and extracted with dichloromethane (3 × 5 ml). The combined organic layers were washed with a saturated solution of NaHCO₃ (1 × 10 ml) and dried over anhydrous sodium sulphate. The reaction mixture was then concentrated by evaporation and the crude product was purified by column chromatography (silica gel 60–120 mesh) by using ethyl acetate in hexane as an eluent to afford the desired product **10**.

Conflicts of interest

The authors declare no conflicts of interest.

Acknowledgements

We would like to thank Science & Engineering Research Board (SERB, EMR/2016/005089 dated 30.6.2017), Department of Chemistry, North-Eastern Hill University (NEHU) for financial support, and the University Grant Commission (UGC) for the Non-Net Fellowship. We are thankful to Sophisticated Analytical and Instrumentation Facility (SAIF) of North Eastern Hill University, Shillong, Department of Chemistry, IIT-Guwahati and Institute Instrumentation centre, IIT-Roorkee. We also acknowledge Central Instruments Facility (CIF) of NIPER, Guwahati for their assistance with GC-MS analysis.

References

- 1 A. Balanta, C. Godard and C. Claver, *Chem. Soc. Rev.*, 2011, **40**, 4973–4985.
- 2 (a) B. F. Mohazzab, B. Jaleh, M. Nasrollahzadeh and Z. Issaabadi, *Catal. Lett.*, 2019, **149**, 169–179; (b) V. V. Namboodiri and R. S. Varma, *Green Chem.*, 2001, **3**, 146–148.
- 3 R. Andrés, E. Jesús and J. C. Flores, *New J. Chem.*, 2007, **31**, 1161–1191.
- 4 T. Kamiguchi, R. Sakazaki, K. Nagashima, Y. Kawamura, Y. Yasuda, K. Matsushima, H. Tani, Y. Takahashi, K. Ishii, R. Suzuki, K. Koizumi, H. Nakai, Y. Ikenishi and Y. Terui, *J. Antibiot.*, 1998, **51**, 445–450.
- 5 (a) T. Norikura, K. Fujiwara, T. Yanai, Y. Sano, T. Sato, T. Tsunoda, K. Kushibe, A. Todate, Y. Morinaga, K. Iwai and H. Matsue, *J. Agric. Food Chem.*, 2013, **61**, 1258–1264; (b) S. Cai, S. Sun, H. Zhou, X. Kong, T. Zhu, D. Li and Q. Gu, *J. Nat. Prod.*, 2011, **74**, 1106–1110; (c) J. Qiu, B. Zhao, Y. Shen, W. Chen, Y. Ma and Y. Shen, *Eur. J. Med. Chem.*, 2013, **68**, 192–202.
- 6 I.-K. Lee, B.-S. Yun, J.-P. Kim, I.-J. Ryoo, Y.-H. Kim and I.-D. Yoo, *Biosci., Biotechnol., Biochem.*, 2003, **67**, 1813–1816.
- 7 (a) T. Norikura, K. Fujiwara, T. Narita, S. Yamaguchi, Y. Morinaga, K. Iwai and H. Matsue, *J. Agric. Food Chem.*, 2011, **59**, 6974–6979; (b) T. Norikura, K. Fujiwara, T. Yanai, Y. Sano, T. Sato, T. Tsunoda, K. Kushibe, A. Todate,

- Y. Morinaga, K. Iwai and H. Matsue, *J. Agric. Food Chem.*, 2013, **61**, 1258–1264.
- 8 (a) W. Yan, Wuringege, S.-J. Li, Z.-K. Guo, W.-J. Zhang, W. Wei, R.-X. Tan and R.-H. Jiao, *Bioorg. Med. Chem. Lett.*, 2017, **27**, 51–54; (b) W. Li, W. Gao, M. Zhang, Y.-L. Li, L. Li, X.-B. Li, W.-Q. Chang, Z.-T. Zhao and H.-X. Lou, *J. Nat. Prod.*, 2016, **79**, 2188–2194.
- 9 A. Takahashi, R. Kudo, G. Kusano and S. Nozoe, *Chem. Pharm. Bull.*, 1992, **40**, 3194–3196.
- 10 (a) S. Casalini, M. Berto, F. Leonardi, A. Operamolla, C. A. Bortolotti, M. Borsari, W. Sun, R. D. Felice, S. Corni, C. Albonetti, O. H. Omar, G. M. Farinola and F. Biscarini, *Langmuir*, 2013, **29**, 13198–13208; (b) F. Maya and J. M. Tour, *Tetrahedron*, 2004, **60**, 81–92.
- 11 (a) T. E. Barder, S. D. Walker, J. R. Martinelli and S. L. Buchwald, *J. Am. Chem. Soc.*, 2005, **127**, 4685–4696; (b) A. F. Littke and G. C. Fu, *Angew. Chem., Int. Ed.*, 2002, **41**, 4176–4211; (c) S. Chatterjee and S. K. Bhattacharya, *ACS Omega*, 2018, **3**, 12905–12913; (d) L. Liu, Y. Zhang and B. Xin, *J. Org. Chem.*, 2006, **71**, 3994–3997; (e) Y. Han, J.-Q. Di, A.-D. Zhao and Z.-H. Zhang, *Appl. Organomet. Chem.*, 2019, **33**, e5172; (f) M. Akkoç, N. Bugday, S. Altın and S. Yasar, *Appl. Organomet. Chem.*, 2021, **35**, e6233; (g) D. Nagai, M. Morita and T. Yamanobe, *ACS Omega*, 2020, **5**, 18484–18489; (h) W. Xu, C. Liu, D. Xiang, Q. Luo, Y. Shu, H. Lin, Y. Hu, Z. Zhang and Y. Ouyang, *RSC Adv.*, 2019, **9**, 34595–34600; (i) P. Chatelain, A. Sau, C. N. Rowley and J. Moran, *Angew. Chem., Int. Ed.*, 2019, **58**, 14959–14963; (j) C. M. So, C. P. Lau, A. S. C. Chan and F. Y. Kwong, *J. Org. Chem.*, 2008, **73**, 7731–7734.
- 12 A. Roglans, A. Pla-Quintana and M. Moreno-Manas, *Chem. Rev.*, 2006, **106**, 4622–4643.
- 13 (a) S. Darses, T. Jeffery, J.-P. Genet, J.-L. Brayer and J.-P. Demoute, *Tetrahedron Lett.*, 1996, **37**, 3857–3860; (b) S. Darses, T. Jeffery, J.-L. Brayer, J.-P. Demoute and J.-P. Genet, *Bull. Soc. Chim. Fr.*, 1996, **133**, 1095–1102; (c) S. Darses, J.-P. Genet, J.-L. Brayer and J.-P. Demoute, *Tetrahedron Lett.*, 1997, **38**, 4393–4396; (d) S. Darses, G. Michaud and J.-P. Genet, *Tetrahedron Lett.*, 1998, **39**, 5045–5048; (e) S. Darses, G. Michaud and J.-P. Genet, *Eur. J. Org. Chem.*, 1999, 1875–1883.
- 14 (a) F.-X. Felpin, E. Fouquet and C. Zakri, *Adv. Synth. Catal.*, 2008, **350**, 2559–2565; (b) F.-X. Felpin, E. Fouquet and C. Zakri, *Adv. Synth. Catal.*, 2009, **351**, 649–655; (c) F. L. Callonnet, E. Fouquet and F.-X. Felpin, *Org. Lett.*, 2011, **13**, 2646–2649.
- 15 (a) J. W. B. Fyfe, N. J. Fazakerley and A. J. B. Watson, *Angew. Chem., Int. Ed.*, 2017, **56**, 1249–1253; (b) P. Cotugno, A. Monopoli, F. Ciminale, N. Cioffi and A. Nacci, *Org. Biomol. Chem.*, 2012, **10**, 808–813.
- 16 (a) F. Beaumard, P. Dauban and R. H. Dodd, *Org. Lett.*, 2009, **11**, 1801–1804; (b) S. A. Kazi, E. M. Campi and M. T. W. Hearn, *Tetrahedron*, 2018, **74**, 1731–1741.
- 17 R. H. Taylor and F.-X. Felpin, *Org. Lett.*, 2007, **9**, 2911–2914.
- 18 X. Li, C. Liu, L. Wang, Q. Ye, X. Jin and Z. Jin, *Org. Biomol. Chem.*, 2018, **16**, 8719–8723.
- 19 Y. B. Platonova, A. N. Volov and L. G. Tomilova, *J. Catal.*, 2019, **373**, 222–227.
- 20 H. Li, Z. Zhu, J. Liu, S. Xie and H. Li, *J. Mater. Chem.*, 2010, **20**, 4366–4370.
- 21 A. Komaromi, G. L. Tolnai and Z. Novak, *Tetrahedron Lett.*, 2008, **49**, 7294–7298.
- 22 J. T. Guan, T. Q. Weng, G.-A. Yu and S. H. Liu, *Tetrahedron Lett.*, 2007, **48**, 7129–7133.
- 23 J. González-Rivera, I. R. Galindo-Esquivel, M. Onor, E. Bramanti, I. Longoc and C. Ferrari, *Green Chem.*, 2014, **16**, 1417–1425.
- 24 T. Kawasaki, Y. Araki, K. Hatase, K. Suzuki, A. Matsumoto, T. Yokoi, Y. Kubota, T. Tatsumi and K. Soa, *Chem. Commun.*, 2015, **51**, 8742–8744.
- 25 S. Zhang, C.-R. Chang, Z.-Q. Huang, J. Li, Z. Wu, Y. Ma, Z. Zhang, Y. Wang and Y. Qu, *J. Am. Chem. Soc.*, 2016, **138**, 2629–2637.
- 26 H. Kaur, D. Shah and U. Pal, *Catal. Commun.*, 2011, **12**, 1384–1388.
- 27 (a) L. He, K. Natte, J. Rabeah, C. Taeschler, H. Neumann, A. Brckner and M. Beller, *Angew. Chem., Int. Ed.*, 2015, **54**, 4320–4324; (b) M. Cai, Q. Xu and Y. Huang, *J. Mol. Catal. A: Chem.*, 2007, **271**, 93–97.
- 28 B. Yuan, Y. Pan, Y. Li, B. Yin and H. Jiang, *Angew. Chem., Int. Ed.*, 2010, **49**, 4054–4058.
- 29 (a) P. Serp, M. Corrias and P. Kalck, *Appl. Catal., A*, 2003, **253**, 337–358; (b) X. Hu, L. Lei, H. P. Chu and P. L. Yue, *Carbon*, 1999, **37**, 631–637; (c) M.-Y. Yen, C.-C. Teng, M.-C. Hsiao, P.-I. Liu, W.-P. Chuang, C.-C. M. Ma, C.-K. Hsieh, M.-C. Tsai and C.-H. Tsai, *J. Mater. Chem.*, 2011, **21**, 12880–12888; (d) V. Georgakilas, J. N. Tiwari, K. C. Kemp, J. A. Perman, A. B. Bourlinos, K. S. Kim and R. Zboril, *Chem. Rev.*, 2016, **116**, 5464–5519; (e) A. Goswami, A. K. Rathi, C. Aparicio, O. Tomanec, M. Petr, R. Pocklanova, M. B. Gawande, R. S. Varma and R. Zboril, *ACS Appl. Mater. Interfaces*, 2017, **9**, 2815–2824.
- 30 S. Moussa, A. R. Siamaki, B. F. Gupton and M. S. El-Shall, *ACS Catal.*, 2011, **2**, 145–154.
- 31 A. R. Siamaki, A. E. R. S. Khder, V. Abdelsayed, M. S. El-Shall and B. F. Gupton, *J. Catal.*, 2011, **279**, 1–11.
- 32 S. K. Movahed, M. Dabiri and A. Bazgir, *Appl. Catal., A*, 2014, **488**, 265–274.
- 33 H. Veisia, T. Tamoradia, B. Karmakar, P. Mohammadi and S. Hemmati, *Mater. Sci. Eng., C*, 2019, **104**, 109919.
- 34 (a) R. Jamatia, A. Gupta, B. Dam, M. Saha and A. K. Pal, *Green Chem.*, 2017, **19**, 1576–1585; (b) S. Santra, P. K. Hota, R. Bhattacharyya, P. Bera, P. Ghosh and S. K. Mandal, *ACS Catal.*, 2013, **3**, 2776–2789; (c) B. Paulchamy, G. Arthi and B. D. Lignesh, *J. Nanomed. Nanotechnol.*, 2015, **6**, 1–4; (d) M. Kamalanathan and R. Gopalakrishnan, *Solid State Phys.*, 2015, **1665**, 120038.
- 35 (a) V. Kumar, S. Srivastava, S. Umrao, R. Kumar, G. Nath, G. Sumana, P. S. Saxena and A. Srivastava, *RSC Adv.*, 2014, **4**, 2267–2273; (b) B.-H. Kim, S.-H. Lee, S.-W. Han, S. Ahn, J. Noh and J. B. Park, *Mater. Express*, 2016, **6**, 61–68.
- 36 (a) R. Sarkar, B. Dam, L. Kyndiah, F. K. Sarkar, S. Gajurel and A. K. Pal, *Green Chem.*, 2022, **24**, 5579–5591; (b) Q. Zhang, Z. Mao, K. Wang, N. T. S. Phan and

- F. Zhang, *Green Chem.*, 2020, **22**, 3239–3247; (c) T. Tene, G. T. Usca, M. Guevara, R. Molina, F. Veltri, M. Arias, L. S. Caputi and C. V. Gomez, *Nanomaterials*, 2020, **10**, 279.
- 37 Z. Cui and X. Bai, *Ultrason. Sonochem.*, 2021, **70**, 105309.
- 38 T. Soltani and B.-K. Lee, *J. Colloid Interface Sci.*, 2017, **486**, 337–343.
- 39 (a) R. Tomar, N. Singh, N. Kumar, V. Tomar and R. Chandra, *Catal. Lett.*, 2019, **149**, 1589–1594; (b) M. Mirza-Aghayan, M. Mohammadi, A. Addad and R. Boukherroub, *Appl. Organomet. Chem.*, 2020, **34**, e5524; (c) Z. Cuia and X. Baia, *Ultrason. Sonochem.*, 2021, **70**, 105309.
- 40 A. P. Colleville, R. A. J. Horan and N. C. O. Tomkinson, *Org. Process Res. Dev.*, 2014, **18**, 1128–1136.
- 41 T. N. Glasnova and C. O. Kappe, *Adv. Synth. Catal.*, 2010, **352**, 3089–3097.
- 42 (a) N. Salarinejad, M. Dabiri and S. K. Movahed, *Colloid Interface Sci. Commun.*, 2022, **47**, 100606; (b) P. Pachfule, M. K. Panda, S. Kandambeth, S. M. Shivaprasad, D. Díaz and R. Banerjee, *J. Mater. Chem. A*, 2014, **2**, 7944–7952.
- 43 J. M. Bhojane, S. A. Sarode and J. M. Nagarkar, *New J. Chem.*, 2016, **40**, 1564–1770.
- 44 L. Geng, Y. Li, Z. Qi, H. Fan, Z. Zhou, R. Chen, Y. Wang and J. Huang, *Catal. Commun.*, 2016, **82**, 24–28.
- 45 M. Gholinejad, F. Zareh and C. Nájera, *Appl. Organomet. Chem.*, 2018, **32**, e3984.
- 46 Y. Liu, J. Wang, T. Li, Z. Zhao and W. Pang, *Tetrahedron*, 2019, **75**, 130540.
- 47 D. Guo, W. Shi and G. Zou, *Adv. Synth. Catal.*, 2022, **364**, 2438–2442.
- 48 J.-Y. Zhou, R.-Q. Liu, C.-Y. Wang and Y.-M. Zhu, *J. Org. Chem.*, 2020, **21**, 14149–14157.
- 49 S. Bunda, A. Udvardy, K. Voronova and F. Joo, *J. Org. Chem.*, 2018, **83**, 15486–15492.
- 50 E. Turunç, S. Akay, T. Baran, D. Kalderis, T. Tsubota and B. Kayan, *New J. Chem.*, 2021, **45**, 12519–12527.
- 51 J.-C. Wang, C.-X. Liu, X. Kan, X.-W. Wu, J.-L. Kana and Y.-B. Dong, *Green Chem.*, 2020, **22**, 1150–1155.
- 52 K. Manna and R. Jana, *Org. Lett.*, 2023, **25**, 341–346.
- 53 Y. Du, S. Wei, M. Tang, M. Ye, H. Tao, C. Qi and L. Shao, *Appl. Organomet. Chem.*, 2020, **34**, e5619.
- 54 F. Aryanassab, M. Shabaniyan, F. Laoutid and H. Vahabi, *Appl. Organomet. Chem.*, 2021, **35**, e6198.
- 55 F. Valentini, L. Carpisassi, A. Comes, C. Aprile and L. Vaccaro, *ACS Sustainable Chem. Eng.*, 2022, **10**, 12386–12393.
- 56 W. Xu, C. Liu, D. Xiang, Q. Luo, Y. Shu, H. Lin, Y. Hu, Z. Zhang and Y. Ouyang, *RSC Adv.*, 2019, **9**, 34595–34600.
- 57 M. A. Ashraf, Z. Liu, C. Li and D. Zhang, *Catal. Lett.*, 2021, **151**, 2207–2222.
- 58 (a) W. S. Hummers and R. E. Offeman, *J. Am. Chem. Soc.*, 1958, **80**, 1339; (b) K.-H. Liao, A. Mittal, S. Bose, C. Leighton, K. A. Khoyan and C. W. Macosko, *ACS Nano*, 2011, **5**, 1253–1258.